Proceedings of the 2024 IEEE
International Conference on Robotics and Biomimetics
December 10-14, 2024, Bangkok, Thailand

Design, Manufacturing, and Control of a Cable-Driven Bionic Robotic Hand

Chunhin Lai, Shuai Liu, Molong Duan*

***Abstract*— This paper details the design, manufacturing, and control of a cable-driven bionic robotic hand that closely mimics human hand movements while addressing the limitations of existing robotic hands such as high weight, size, and cost. By optimizing degrees of freedom and employing advanced fabrication methods, a solution of lightweight, cost-effective model that maintains high functionality is presented. The hand employs a cable-driven system to improve dexterity and reduce complexity, making it suitable for applications in healthcare, manufacturing, and prosthetics. The system's performance is evaluated in terms of workspace, object grasping, and free-space motion.**

Keywords—robotics, bionic hand, cable-driven, control

I. Introduction

The development of robotic hands has garnered significant attention as a versatile solution across various sectors, including medical robotics [1] [2], healthcare [3], and manufacturing [4]. These advanced systems are designed to emulate the functionality and agility of the human hand, which is crucial for a broad spectrum of tasks, from surgical support to prosthetic applications and automated manufacturing processes. A standard biomimetic robotic hand replaces the human hand's ligaments and tendons with elastic components and cables, thus creating a mechanical framework closely resembling natural hand movements [5].

One of the main challenges in this domain is to achieve these intricate movements with a minimal number of actuators while still ensuring a high degree of dexterity and grasping strength. As depicted in Fig. 1, the human hand possesses 17 distinct knuckles, which presents a formidable challenge in the design of a lightweight and robust anthropomorphic robotic hand. The complexity lies in the difficulty of integrating multiple actuators and sensors into a compact design [6]. To overcome these challenges, many robotic hands incorporate a four-bar linkage mechanism at the proximal interphalangeal (PIP) and distal interphalangeal (DIP) joints, facilitating synchronized motion between these joints [7]. Furthermore, recent research has seen considerable advancements in the design and control of cable-driven robotic hands. For instance, Mountain et al. [8] introduced a force control algorithm utilizing Youla parameterization and iterative learning control, which has enhanced grasping performance. Min et al. [9] proposed a parallel cable-driven hand capable of adaptive grasping. Similarly, Nikafrooz et al. [10] presented a single-actuated, cable-driven hand that, while reducing complexity and weight, compromises dexterity and control precision due to its under-actuated nature. Additionally, Li et al. [12] developed a 3D-printed, lightweight robotic hand with an integrated design, which simplifies the manufacturing process but restricts scalability and flexibility due to its rigid architecture. However, most of these existing designs suffer from a lack of modularity, complicating maintenance and adaptability.

*Molong Duan is with Hong Kong University of Science and Technology, Hong Kong SAR, China, as well as HKUST Shenzhen-Hong Kong Collaborative Innovation Research Institute, Futian, Shenzhen, China (corresponding author, phone: (852) 3469 3024; e-mail: duan@ust.hk). author, phone: (852) 3469 3024; e-mail: duan@ust.hk).

Chunhin Lai and Shuai Liu are with Hong Kong University of Science and Technology, Hong Kong SAR, China (e-mails: chlaias@connect.ust.hk, sliucr@connect.ust.hk).

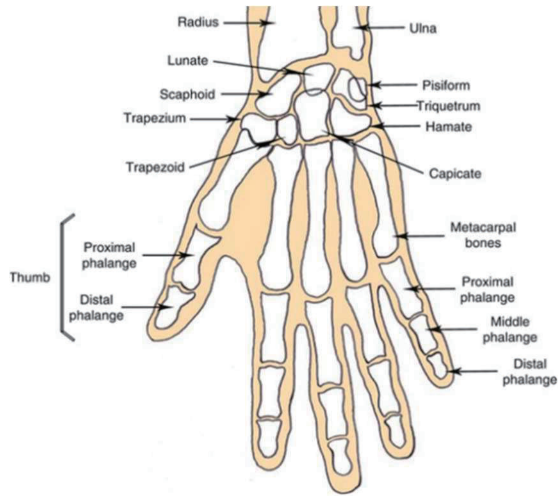

Fig. 1. Human hand anatomy [11]

To address these limitations, a modular, cable-driven bionic hand that retains high dexterity with fewer actuators is designed in this paper. This design emphasizes scalability and ease of maintenance, allowing for more efficient system adaptation. The contributions of the paper are:

- A cable-driven bionic robotic hand (CDBRH) which reduces degrees of freedom while maintaining complex motions, offering a more efficient and functional solution than existing robotic hands, is designed and manufactured;
- A scalable, modular design approach is introduced to simplify maintenance and enhance system adaptability;
- The proposed design and control methods have been experimentally verified.

The remainder of this paper is structured as follows: Section II describes the mechanical design, focusing on the structural components and materials used. Section III presents the modelling and control of the cable-driven bionic hand. Section IV outlines the experimental setup and results, evaluating the performance of the proposed design. Finally, Section V concludes the paper and discusses future work.

II. Mechanical Design of the CDBRH

The primary goal of bionic robotic hand design is to closely replicate the functionality and dexterity of a human hand while addressing key limitations found in existing robotic hands, such as excessive weight, size, and cost. To achieve this, the design is grounded in the principles of human hand anatomy and biomechanics, prioritizing lightweight materials, optimized DOF, and a simplified actuation system. The use of a cable-driven mechanism is central to this approach, as it reduces the complexity of the control system and minimizes the number of actuators required, while still providing sufficient dexterity for a wide range of applications. There are a few main components that form the complete hand assembly, including the fingers, palm, and limb. The finger design is based on the bone structure of the human hand, as shown in Fig. 1. The bionic hand is simplified into a design with 12 DOF, as Fig. 2 shows. The palm serves multiple functions: guiding cables to the fingers, facilitating finger adduction, and restricting finger movement. The limb houses the motors and arranges the cables before they pass through the palm. The overall structure of the CDBRH is shown in Fig. 3.

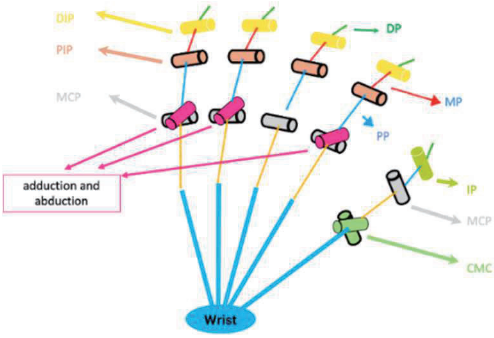

Fig. 2. Schematics of cable-driven bionic hand design

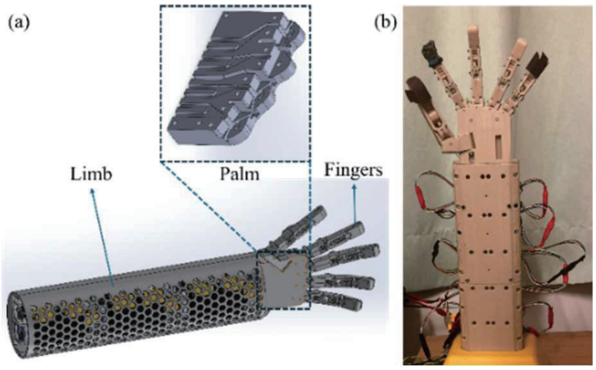

Fig. 3. (a) Design and (b) prototype of the overall robotic hand structure

A. Fingers of CDBRH

The bionic hand design reduces each finger's DOF from 4 to 3. Each finger consists of four main parts: the Distal phalange (TIP), Middle phalange (MLP), Proximal phalange (PLP), and knuckles. For the thumb, additional components, such as the trapezium, trapezoid (TRP), are included due to its unique geometry and motion. The fingers are actuated by motors pulling cables, allowing for both bending and extension movements. To bend the finger, the motor pulls the cable, illustrated by the red line l_4 in Fig. 4. To extend the finger, the other cable l_3 is pulled.

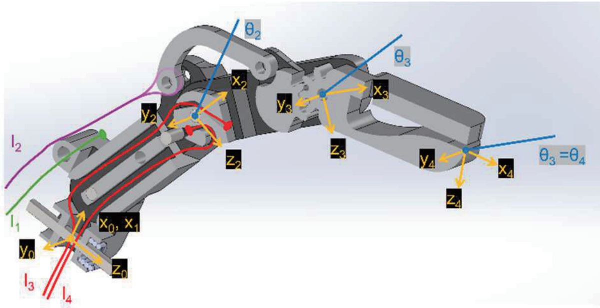

Fig. 4. Frames assignment and cable deployment of a single finger

B. Palm of CDBRH

In human anatomy, adduction and abduction describe the movement of the fingers toward and away from the midline of the hand, respectively. These movements allow for a wide range of tasks, from gripping objects to more delicate maneuvers. While each finger can move independently, they often work together, particularly during tasks that involve flexion and extension. As illustrated in Fig. 5, the middle finger remains steady during adduction and abduction. To simplify the control mechanism, the MCP joints of each finger are reduced to 1 DOF, with a single cable controlling adduction and elastic bands passively aiding abduction. Bearings are used as idler pulleys to minimize friction during cable routing inside the palm. These bearings guide the cables from the fingers to the limb, ensuring smooth movement and avoiding collisions.

C. Limb of CDBRH

The cables are pre-arranged before passing through the palm to minimize friction between the cables and the hand's main structure. This is achieved using pulley systems and Teflon tubes that are snap-fit onto the limb, with the cable layout specifically arranged to enhance efficiency and minimize friction, as shown in Fig. 6 (a).

D. Material and component consideration of CDBRH

The driver board is mounted on the motor array using a 3D-printed mount created through Fused Deposition Modelling (FDM). Table I shows the corresponding cable and joint control of motors, and each motor control the corresponding pulley angle ϕ_i. For parts without high heat exposure, Polylactide (PLA) is used due to its cost-effectiveness. However, for the driver board mount, an acrylic plate is used due to its higher heat resistance, as shown in Fig. 6 (b).

Fig. 5. Schematics of adduction and abduction

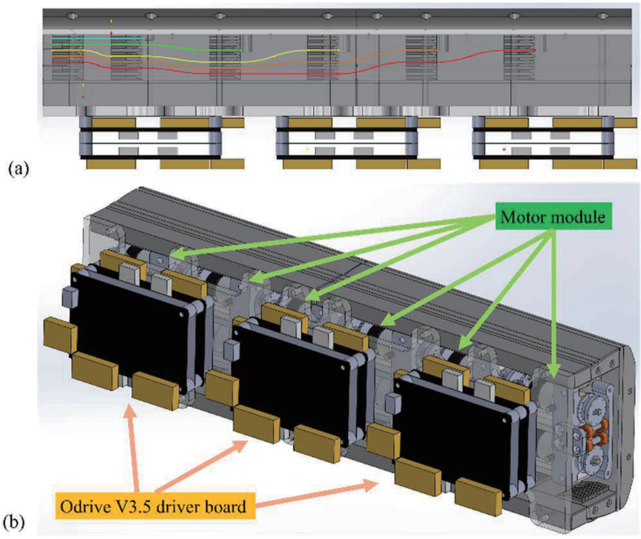

Fig. 6. (a) Cable layout in the limb, and (b) Isotropic view of limb

Table I. Motor Characteristic of CDBRH

Appearance		
	Input voltage	4-8V
	Stall current	5A
	Stall torque	1.11Nm (with gearbox)
	Gear ratio	1:100
	Weight	9 grams

The Brushless Direct Current (BLDC) motor has been selected as the actuator for our cable-driven system for its robustness and high power density [13]. The absence of brushes and commutators in its structure significantly contributes to its longevity by reducing wear and potential failure points. Additionally, BLDC motors provide the advantage of integrated torque feedback derived from the current supplied, which can be described as:

$$T_{motor} = \frac{60}{2\pi K_v} I_{applied}, \tag{1}$$

where T_{motor} represents the motor torque, K_v denotes the motor's velocity constant, and $I_{applied}$ is the applied current. These properties make BLDC motors particularly suitable for applications where monitoring cable tension is crucial, such as in our system. Specifically, we use a 1104 BLDC motor combined with an N20 series gearbox as depicted in Table II. This choice of motor and gearbox not only meets our torque requirements but also simplifies the system design by reducing space and complexity. To further optimize the form factor and weight, the motor is integrated into a module, with a custom PCB encoder using a rotary magnetic sensor IC, AS5047P. This choice is more applicable compared to sensors such as rotary capacitive sensors, as it helps maintain a compact and lightweight design. This modular design is mount on limb using screw holes which provide an efficient way to replace component for simplistic disassembling procedure.

Nylon fishing wire is used as cable for high flexibility and smooth movement, which are crucial for replicating natural finger motion. Its low friction properties enhance force transmission efficiency. Additionally, nylon fishing wire is cost-effective and readily available, aligning with our goal of affordability. Its flexible nature allows for precise control of finger positions through the adjustment of cable tensions, making it the optimal choice for our design.

Table II. Motor configuration of CDBRH

Motor	**Direct linked**	**Indirect linked**	**Motor**	**Direct linked**	**Indirect linked**
1	$\theta_{3,little}$	$\theta_{4,little}$	2	$\theta_{3,ring}$	$\theta_{4,ring}$
3	$\theta_{3,thumb}$	$\theta_{4,thumb}$	4	$\theta_{3,middle}$	$\theta_{4,middle}$
5	$\theta_{1,index}$ $\theta_{1,middle}$ $\theta_{1,ring}$ $\theta_{1,little}$	-	6	$\theta_{2,little}$	-
7	$\theta_{3,index}$	$\theta_{4,index}$	8	$\theta_{2,thumb}$	-
9	$\theta_{2,middle}$	-	10	$\theta_{2,ring}$	-
11	$\theta_{2,index}$	-	12	$\theta_{1,thumb}$	-

III. Modelling and Control

A. *Kinematics of the bionic robotic hand*

The intricate anatomy of the human hand facilitates precise movements and diverse grasping capabilities. Replicating every biological detail in a robotic hand can result in an overly complex design, which is often not ideal. Consequently, the proposed design focuses on emulating hand movements execution, aiming to achieve various grasp types with minimal actuator and sensor input. The schematics of the cable-driven bionic hand is presented in Fig. 2, in which the cylinder represents the rotation joint around its axis. Note that the carpometacarpal (CMC) joint for thumb and the metacarpophalangeal (MCP) joints for index, ring, and little finger are 2 degrees of freedom (DOF) in the proposed structure, similar to the functionality of physical knuckles. The general characteristics of the robotic hand are shown in Table III.

Table III. General characteristic of the robotic hand

Weight (g)	**No. of joints**	**DOF**	**No. of actuators**
850	12	20	12

Since the cables pass through one or more joints, the control of each motor is not independent. Fig. 4 has shown the finger configuration and frame assignment in one finger, with the MCP joint divided into 2 separate joints (MCP1 and MCP2). Considering the fingertip as the endpoint, the frames F_i are assigned as:

- F_0 : MCP1,
- F_1 : MCP2,
- F_2 : PIP,
- F_3 : DIP,
- and F_4 : Fingertip.

The kinematics of the finger is described using Denavit-Hartenberg (DH) parameters, as shown in Table IV, with the phalange length and the kinematic range of each joint shown in Table V. Note that the MCP joint of the middle finger has a range of 0 for adduction and abduction, as these movements are accommodated by the other fingers.

Based on the established kinematics, the position and orientation of the fingertip P_{tip} of non-thumb finger with respect to the base reference at F_0 could thus be determined by forward kinematics:

$$P_{tip}=\begin{bmatrix} c_1(a_1+a_2c_2+a_3c_{23}+a_4c_{234}) \\ s_1(a_1+a_2c_2+a_3c_{23}+a_4c_{234}) \\ a_2s_2+a_3s_{23}+a_4s_{234} \end{bmatrix}, \quad (2)$$

where, $c_i=\cos(\theta_i)$, $s_i=\sin(\theta_i)$, $c_{23}=\cos(\theta_2+\theta_3)$, $s_{23}=\sin(\theta_2+\theta_3)$, $s_{234}=\sin(\theta_2+\theta_3+\theta_4)$, and $c_{234}=\cos(\theta_2+\theta_3+\theta_4)$. For the thumb finger:

$$P_{thumb}=\begin{bmatrix} a_2M_{12}+a_3M_{13}+a_4M_{14}+a_5M_{15} \\ a_2M_{22}+a_3M_{23}+a_4M_{24}+a_5M_{25} \\ a_2M_{32}+a_3M_{33}+a_4M_{34}+a_5M_{35} \end{bmatrix}, \quad (3)$$

where,

$$\begin{aligned}
&M_{12}=c_{\theta_1}c_{\theta_2}, M_{13}=s_{\theta_1}s_{\theta_3}+c_{\theta_1}c_{\theta_2}c_{\theta_3},\\
&M_{14}=s_{\theta_1}s_{\theta_3}+c_{\theta_1}c_{\theta_2}c_{\theta_3}c_{\theta_4}+c_{\theta_1}s_{\theta_2}s_{\theta_4},\\
&M_{15}=c_{\theta_1}c_{\theta_2}c_{\theta_3}c_{\theta_4}c_{\theta_5}+s_{\theta_1}s_{\theta_3}c_{\theta_4}c_{\theta_5}+c_{\theta_1}s_{\theta_2}s_{\theta_4}c_{\theta_5}\\
&\quad -c_{\theta_1}c_{\theta_2}c_{\theta_3}s_{\theta_4}s_{\theta_5}-s_{\theta_1}s_{\theta_3}s_{\theta_4}s_{\theta_5}-c_{\theta_1}s_{\theta_2}c_{\theta_4}s_{\theta_5},\\
&M_{22}=s_{\theta_1}c_{\theta_2}, M_{23}=c_{\theta_1}s_{\theta_3}+s_{\theta_1}c_{\theta_2}c_{\theta_3},\\
&M_{24}=s_{\theta_1}s_{\theta_2}s_{\theta_4}+s_{\theta_1}c_{\theta_2}c_{\theta_3}c_{\theta_4}-c_{\theta_1}s_{\theta_3}c_{\theta_4}, \qquad (4)\\
&M_{25}=s_{\theta_1}c_{\theta_2}c_{\theta_3}c_{\theta_4}c_{\theta_5}+s_{\theta_1}s_{\theta_2}s_{\theta_4}c_{\theta_5}+c_{\theta_1}s_{\theta_3}s_{\theta_4}s_{\theta_5}\\
&\quad +s_{\theta_1}s_{\theta_2}c_{\theta_4}s_{\theta_5}-c_{\theta_1}s_{\theta_3}c_{\theta_4}c_{\theta_5}-s_{\theta_1}c_{\theta_2}c_{\theta_3}s_{\theta_4}s_{\theta_5},\\
&M_{32}=s_{\theta_2}, M_{33}=s_{\theta_2}c_{\theta_3}, M_{34}=s_{\theta_2}c_{\theta_3}c_{\theta_4}+c_{\theta_2}s_{\theta_4},\\
&M_{35}=s_{\theta_2}c_{\theta_3}c_{\theta_4}c_{\theta_5}-s_{\theta_2}c_{\theta_3}s_{\theta_4}s_{\theta_5}\\
&\quad -c_{\theta_2}c_{\theta_4}s_{\theta_5}-c_{\theta_2}s_{\theta_4}c_{\theta_5}.
\end{aligned}$$

B. *Motor reference command generation*

Each finger is actuated by three cables, each serving distinct roles in controlling the finger's movements, as shown in Fig. 4. Since the structure of the finger joints remains unchanged, the length of the cable (l_i) changes linearly with the joint angles (θ_i), which can be expressed as

$$l_i=\begin{bmatrix} l_1 \\ l_2 \\ l_3 \\ l_4 \end{bmatrix}=\begin{bmatrix} r_1 & 0 & 0 \\ r_2 & 0 & 0 \\ 0 & -r_3 & -r_4 \\ 0 & r_3 & r_4 \end{bmatrix}\begin{bmatrix} \theta_1 \\ \theta_2 \\ -\theta_3 \\ \theta_3 \end{bmatrix}=A\theta_i, \quad (5)$$

$$\frac{\phi_{m,i}}{\mu}=\phi_{p,i}\ ,\ r_{p,i}\phi_{p,i}=l_i, \quad (6)$$

where r_i are non-zero constants, and matrix A is a coupling matrix which describes the relationship between inputs (cable displacements l_i) and outputs (joint displacements θ_i) in the robotic finger mechanism system. The gear ratio is denoted as μ, the cable displacement l_i could be obtained by multiplying the rotational angle of pulley $\phi_{p,i}$ and the radius of pulley $r_{p,i}$. Noted that angle of pulley is calculated by angle of motor divided by gear ratio. Hence, motor reference command, which is proportional to the cable displacements, can be generated using (5) and (6) to regulate the finger posture. Cable l_1 is corresponded to adduction and abduction motion θ_1 which is a combination of four $\theta_{1,n}$ for non-thumb fingers, and is written as:

$$\theta_1=[\theta_{1,2}\ \ \theta_{1,3}\ \ \theta_{1,4}\ \ \theta_{1,5}]. \quad (7)$$

Cable l_2 is corresponded to MLP motion θ_2. By opposing the force provided by torsion installed in the joint, the corresponding motion can be achieved. Cable l_3 and l_4 are installed in the same pulley in opposite direction, which is shown in Fig. 4, providing the actuation and retraction motion of PLP θ_3. Noted that the motion of DIP θ_4 is interrelated to PLP by the linkages shown in Fig. 4.

Table IV. DH parameters of non-thumb fingers and thumb finger.

(a) non-thumb fingers

Link	a_i	α_i	d_i	θ_i
1	a_1	$\pi/2$	0	θ_1^*
2	a_2	0	0	θ_2^*
3	a_3	0	0	θ_3^*
4	a_4	0	0	θ_3^*

(b) thumb finger

Link	a_i	α_i	d_i	θ_i
0	0	$\pi/2$	0	$5\pi/9$
1	a_1	$\pi/2$	0	θ_1^*
2	a_2	$\pi/2$	0	θ_2^*
3	a_3	0	0	θ_3^*
4	a_4	0	0	θ_3^*

Table V. Kinematics parameters of CDBRH

(a) Phalange length (mm)

	Thumb	Index	Middle	Ring	Little
a_1	24.71	8.75	8.75	8.75	8.75
a_2	17.45	25	35	30	20
a_3	35	25	25	25	25
a_4	35	28.5	28.5	28.5	28.5

(b) Kinematic range of each joint

	Thumb	Index	Middle	Ring	Little
θ_1	[0°,60°]	[-14°,0°]	[0°,0°]	[0°,14°]	[14°,28°]
θ_2	[-74°, -14°]	[0°,90°]	[0°,90°]	[0°,90°]	[0°,90°]
θ_3	[0°,45°]	[0°,90°]	[0°,90°]	[0°,90°]	[0°,90°]
θ_4	[0°,90°]	[0°,90°]	[0°,90°]	[0°,90°]	[0°,90°]

The finger posture is defined by using the established fingertip positions P_{tip} and P_{thumb} as

$$P=\{P_{thumb},P_{tip,2},P_{tip,3},P_{tip,4},P_{tip,5}\}. \quad (8)$$

where $P_{tip,n}$ represents four non-thumb fingers' fingertip position. Each finger and the angle between links is driven by multiple cable as (5) shown.

IV. Experiments and Verification

The overall hardware system of the CDBRH for the verification is illustrated in Fig. 7. The control system is built around a Teensy 4.1 microcontroller under the Arduino framework, chosen for its high clock speed, abundant I/O pins, and powerful processing capabilities, which facilitate both ease of development and future upgrades. ODrive V3.5 motor drivers are connected to the microcontroller via UART. Customized PCB encoders, utilizing the AS5047P module, provide motor feedback for precise control. A PC serves as the interface for command input and powers the microcontroller, while a 12V 3-cell LiPo battery powers the motor drivers. The following sections evaluate the performance of the CDBRH, including workspace, object grasping, and free-space motion.

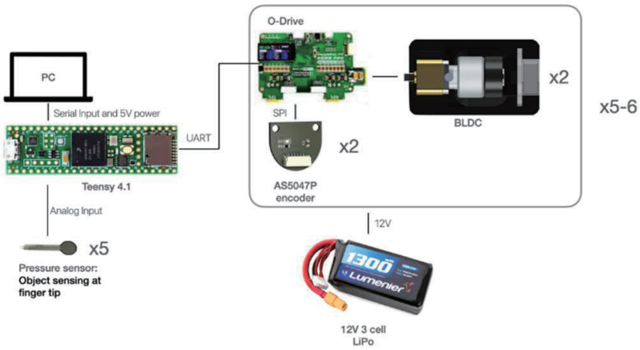

Fig. 7. Hardware system layout of CDBRH

A. Workspace

The workspace analysis provides insights into the capabilities of the robotic hand. MATLAB was used for the calculations and visualization. By applying the DH parameters in Table IV, reachable workspace for each finger was calculated using forward kinematics. From the workspace plots shown in Fig. 8, it can be observed that each finger is able to reach a wide range of workspace, even with reduced degrees of freedom. This indicates that the robotic hand possesses a considerable level of functionality and demonstrates the hand's versatility and dexterity, resulting in the potential for performing complex tasks requiring precise manipulation.

B. Object Grasping

To verify the effectiveness of the control system for the CDBRH, a series of object-grasping experiments were conducted. The goal of these experiments was to assess the hand's ability to accurately perform different types of grasps, simulating industrial use cases. In the experiment, the robotic hand was tasked with grasping two distinct objects: a cylindrical object (stick) and a flat object (card). These two objects were chosen to demonstrate the versatility of the hand's control system in executing different grasp types—power grasp for the stick and precision grasp for the card. To perform these two grasps, joint angles θ_i will be driven by cables l_i and it is shown in Table VI, where $\theta_{n,m}$ representing the n[th] joint displacement of finger m. The results, shown in Fig. 9, illustrate the hand's capability to securely grasp both objects with appropriate grip force and positioning.

C. Free-space motion

In addition to grasping tasks, a free-space motion experiment was conducted to test the versatility and precision of the CDBRH in performing a variety of gestures without interacting with external objects. This experiment aimed to demonstrate the hand's ability to execute complex, human-like motions under the control of the cable-driven system.

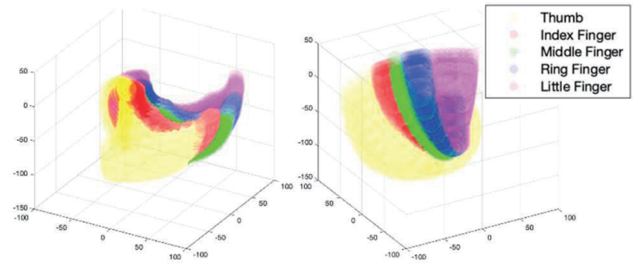

Fig. 8. Fingers Workspace of CDBRH

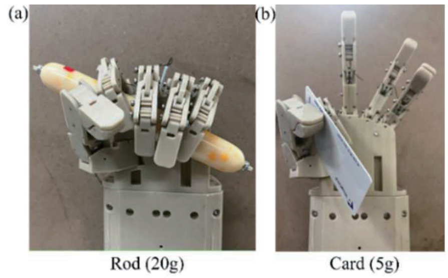

Fig. 9. Object grasp experiment of CDBRH

Table VI. Corresponding object grasping joint angle of:

(a)Rod grasping,

$\theta_{n,1}$	$\theta_{n,2}$	$\theta_{n,3}$	$\theta_{n,4}$	$\theta_{n,5}$
30°	-14°	0°	14°	28°
-74°	90°	90°	90°	90°
45°	90°	90°	90°	90°
90°	90°	90°	90°	90°

(b)Card grasping.

$\theta_{n,1}$	$\theta_{n,2}$	$\theta_{n,3}$	$\theta_{n,4}$	$\theta_{n,5}$
30°	-14°	0°	14°	28°
-74°	90°	0°	0°	0°
45°	90°	0°	0°	0°
90°	90°	0°	0°	0°

During the experiment, the robotic hand was programmed to perform various gestures, including an "OK" gesture, "thumb" signal and "three" signal, as shown in Fig. 10. For the "OK" gesture, the joint angle control is similar to card grasping which is already shown in Table VI (b), and for the others, the corresponding joint angle is shown in Table VII. The successful execution of this gesture, which requires precise control of both the thumb and index finger, highlights the system's capability to achieve fine motor control and replicate human hand dexterity.

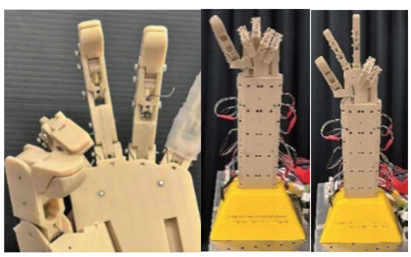

Fig. 10.Free space motion of (a) "OK" signal, (b) "thumb" signal, and (c) signal of "three"

The results from this experiment further validate the control system's ability to coordinate smooth and precise movements across multiple degrees of freedom, demonstrating the hand's potential for applications that require intricate motion control, such as sign language interpretation or fine object manipulation.

Table VII. Corresponding free space motion joint angle of:

(a) "thumb" signal,

$\theta_{n,1}$	$\theta_{n,2}$	$\theta_{n,3}$	$\theta_{n,4}$	$\theta_{n,5}$
0°	-14°	0°	14°	28°
-74°	90°	90°	90°	90°
0°	90°	90°	90°	90°
0°	90°	90°	90°	90°

(b) signal of "three".

$\theta_{n,1}$	$\theta_{n,2}$	$\theta_{n,3}$	$\theta_{n,4}$	$\theta_{n,5}$
0°	-14°	0°	14°	28°
-74°	0°	0°	90°	90°
0°	0°	0°	90°	90°
0°	0°	0°	90°	90°

V. Conclusion

This paper presents a modular, CDBRH that addresses several limitations in existing designs. By reducing the degrees of freedom while maintaining complex finger motions, our design achieves an optimal balance of weight, size, and functionality. The modular and scalable approach simplifies maintenance and enhances system adaptability, overcoming the challenges of repair and component replacement. Additionally, the free-motion control method has been experimentally validated, demonstrating the range of motion and controllability. Future work will focus on utilizing vision-based methods for position compensation to achieve higher precision. Additionally, vision systems will be employed to help record and replicate human hand movements, enabling teleoperation. These developments are expected to further improve the accuracy and adaptability of the robotic hand.

VI. Acknowledgment

The authors would like to thank Materials, Design, and Manufacturing Facility (MDMF) in HKUST for providing the necessary facilities, materials and assistance. In addition, we acknowledge the financial support received from the Department of Mechanical and Aerospace Engineering in HKUST and Mr. Chun Wai KONG for technical hardware and software assistance.

References

[1] A. D.Deshpande *et al.*, "Mechanisms of the Anatomically Correct Testbed Hand," *IEEE/ASME Trans. Mechatronics*, vol. 18, no. 1, pp. 238–250, Feb.2013, doi: 10.1109/TMECH.2011.2166801.

[2] Zhe Xu .Todorov, "Design of a highly biomimetic anthropomorphic robotic hand towards artificial limb regeneration," in *2016 IEEE International Conference on Robotics and Automation (ICRA)*, IEEE, May 2016, pp. 3485–3492. doi: 10.1109/ICRA.2016.7487528.

[3] H.Huang, F.Zhang, L. J.Hargrove, Z.Dou, D. R.Rogers, and K. B.Englehart, "Continuous locomotion-mode identification for prosthetic legs based on neuromuscular-mechanical fusion.," *IEEE Trans. Biomed. Eng.*, vol. 58, no. 10, pp. 2867–75, Oct.2011, doi: 10.1109/TBME.2011.2161671.

[4] A.Billard and D.Kragic, "Trends and challenges in robot manipulation," *Science (80-.).*, vol. 364, no. 6446, Jun.2019, doi: 10.1126/science.aat8414.

[5] J. T.Belter and A. M.Dollar, "Performance characteristics of anthropomorphic prosthetic hands," in *2011 IEEE International Conference on Rehabilitation Robotics*, IEEE, Jun. 2011, pp. 1–7. doi: 10.1109/ICORR.2011.5975476.

[6] J. T.Belter, J. L.Segil, A. M.Dollar, and R. F.Weir, "Mechanical design and performance specifications of anthropomorphic prosthetic hands: A review," *J. Rehabil. Res. Dev.*, vol. 50, no. 5, p. 599, 2013, doi: 10.1682/JRRD.2011.10.0188.

[7] T.Chen, X.Zhao, G.Ma, B.Tao, and Z.Yin, "Design of 3D-printed Cable Driven Humanoid Hand Based on Bidirectional Elastomeric Passive Transmission," *Chinese J. Mech. Eng.*, vol. 34, no. 1, p. 76, Dec.2021, doi: 10.1186/s10033-021-00595-y.

[8] E.Mountain, E.Weise, S.Tian, B.Li, X.Liang, and M.Zheng, "Grasping Force Control and Adaptation for a Cable-Driven Robotic Hand," 2024.

[9] S.Min and S.Yi, "Development of Cable-driven Anthropomorphic Robot Hand," *IEEE Robot. Autom. Lett.*, vol. 6, no. 2, pp. 1176–1183, Apr.2021, doi: 10.1109/LRA.2021.3056375.

[10] N.Nikafrooz and A.Leonessa, "A Single-Actuated, Cable-Driven, and Self-Contained Robotic Hand Designed for Adaptive Grasps," *Robotics*, vol. 10, no. 4, p. 109, Sep.2021, doi: 10.3390/robotics10040109.

[11] S.Gnecchi and F.Moutet, "The Anatomy of the Hand," 2015, pp. 7–32. doi: 10.1007/978-3-319-16790-9_2.

[12] L.Tian, N.Magnenat Thalmann, D.Thalmann, and J.Zheng, "The Making of a 3D-Printed, Cable-Driven, Single-Model, Lightweight Humanoid Robotic Hand," *Front. Robot. AI*, vol. 4, Dec.2017, doi: 10.3389/frobt.2017.00065.

[13] F. A.Kazan and R.Akkaya, "Use of PMSM in Electric Mobility Scooter Propulsion," in *International Conference on Engineering Technologies (ICENTE'19), Konya, Turkey*, 2019.